A Simple 1^+ Dimensional Model of Rowing Mimics Observed Forces and Motions

D. Cabrera [a,*], A. Ruina [a], V. Kleshnev [b]

[a] *Cornell University, Department of Theoretical & Applied Mechanics, Biorobotics & Locomotion Laboratory, Ithaca, NY 14853, USA*

[b] *English Institute of Sport, Bisham Abbey National Sports Centre, Bisham Nr. Marlow, Bucks SL7 1RT, United Kingdom*

Abstract

We have devised a simple, yet predictive model of the mechanics of both sculling and sweep rowing that reasonably mimics observed kinematic and force data. Our physical model is largely based upon the model proposed by Alexander [Alexander, F.H. (1925), "The theory of rowing", *Proceedings of the University of Durham Philosophical Society*, (pp. 160–179)]. The model's primary features include: one dimensional momentum balance, a point mass rower, infinitely stiff oars with inertia and non-infinitesimal stroke angles, and quadratic relationships between force and velocity for the boat and oar blade. Using an inverse dynamics approach, we are able to construct reasonable fits to force and kinematic data of real rowing. We show that the model is able to reasonably well predict boat velocity even when we do not fit for it. A sensitivity analysis shows that the quality of fit is more sensitive to the boat and oar drag coefficients than to other physical parameters. Allowing oar slip ($C_D < \infty$) proves to be a necessary model ingredient but, for example, allowing for oar flexibility does not improve the quality of fit. The model seems to have the key terms and a minimum of superfluous terms for investigations of rowing.

Key words: rowing, model
PACS: 3720

* Corresponding author. Tel.: +1 607 255 7108; fax: +1 607 255 2011
Email addresses: dsc16@cornell.edu (D. Cabrera), ruina@cornell.edu (A. Ruina), kleshnevv@ausport.gov.au (V. Kleshnev).
URL: http://ruina.tam.cornell.edu (A. Ruina).

1 Introduction

Coordination strategies used by competitive rowers seem to be rather stereotypical. Starting in a crouched position with legs fully bent and arms outstretched (a position called *frontstops*), the rower accelerates herself towards the front of the boat, ending in a leaned-back position with legs fully extended and arms fully contracted (a position called *backstops*) by generally sequencing her body motions in the following order: (1) leg extension, (2) back rotation, and (3) arm retraction. The oars are put in the water just after the legs begin to extend and are removed from the water just before the arms are fully retracted. The opposite sequencing (arm extension, back rotation, and leg retraction) is used upon returning to frontstops. Of the many possible coordination patterns one can use to propel a boat, why do rowers tend to use this particular one? If the choice of coordination is determined by optimization, what kind of performance criterion will predict observed rowing patterns? Before getting to this optimization approach one needs a model that can reasonably match observed behavior.

In this paper, we present what we believe to be the most accurate model of rowing to date and which also has minimal complexity. The model is validated for both sculling and sweep rowing using numerical fitting to match on-water force and kinematic data. Hopefully, this model can also be used to answer such questions applicable to rowing as: How can rigging be adjusted for various strength and height rower to row together optimally? Can a moving coxswain make a boat go faster? How much do oar blade properties affect boat speed, etc.?

Previous Research

Starting with Alexander (1925), a handful of attempts have been made to accurately model the mechanics of sculling/sweep rowing. In his model, Alexander assumed one dimensional (1D) mechanics, a point mass rower, an infinitely stiff oar, and quadratic force-velocity relationships to model drag forces on the boat and oar blade. Alexander assumes that the resultant force on the oar blade is perpendicular to the blade and that its magnitude is proportional to the square of the blade's slip velocity (i.e. the component of the blade velocity relative to the water that is perpendicular to the blade). He accounted for the 2D (as viewed from above) kinematics of the oar, the oar's inertia, and also for boat "added-mass" (an effective additional boat mass due to the oscillating kinetic energy of fluid moving around the boat). Alexander prescribed ficticious (but plausible) coordination patterns for the rower's legs, back, and arms as well as the angular velocity of the oar to predict the motions of the system using numerical integration (note the date). Comparison with the scant data

available was somewhat favorable in that there was some agreement with the measured oar handle force profile and with the path traced out by the tip of the oar blade. However, only qualitative kinematics data was available so Alexander did not quantitatively verify his made-up coordination and boat velocity curves.

More recent models resembling those of Alexander have been posed (Pope, 1973; Atkinson, 2004; van Holst, 2004) as well as other simpler models (Sanderson & Martindale, 1986; Millward, 1987; Brearley & de Mestre, 1996; Lazauskas, 1997; Simeoni et al., 2002). See Appendix A.1 for a discussion of these models. With the exception of Atkinson who accurately predicts boat velocity, none of these models is shown to accurately predict observed forces and motions.

2 Methods

2.1 Model Description

The gross features of our model are similar to those of Alexander's. A schematic of the model is shown in Fig. 1. All rowers are assumed to be identical in size, strength, and coordination; they row together in perfect synchrony. For fluid forces we take into account large angular displacements of the oar in a plane parallel to the water surface. We consider leg, back, and arm motions in the fore-aft direction. We neglect the pitching and yawing motions of the boat and assume that the rower keeps the boat balanced using zero effort. In our idealization, the rower's center of mass and shoulder height from the sliding seat are constant, the rower's mass is concentrated in her gut, the oars have inertia and are perfectly rigid oars, the force on the oar blade is normal to the oar axis, the water is still, and there is no air resistance.

2.2 Governing Equations

The model is governed by the laws of classical rigid-body mechanics. Because we assume identical and perfectly synchronous rowers, we analyze the mechanics of a single rower while scaling masses accordingly. We evaluate linear momentum balance for the rower, oar, and boat in the fore-aft direction and angular momentum balance for the oar about the oarlock to determine the equations of motion for each phase of the stroke: *drive* and *recovery*. The *drive* is defined as the portion of the stroke when the oars are in the water while the *recovery* is the remainder of the stroke when the oars are in the air. (Note that this definition differs slightly from the definition of drive and re-

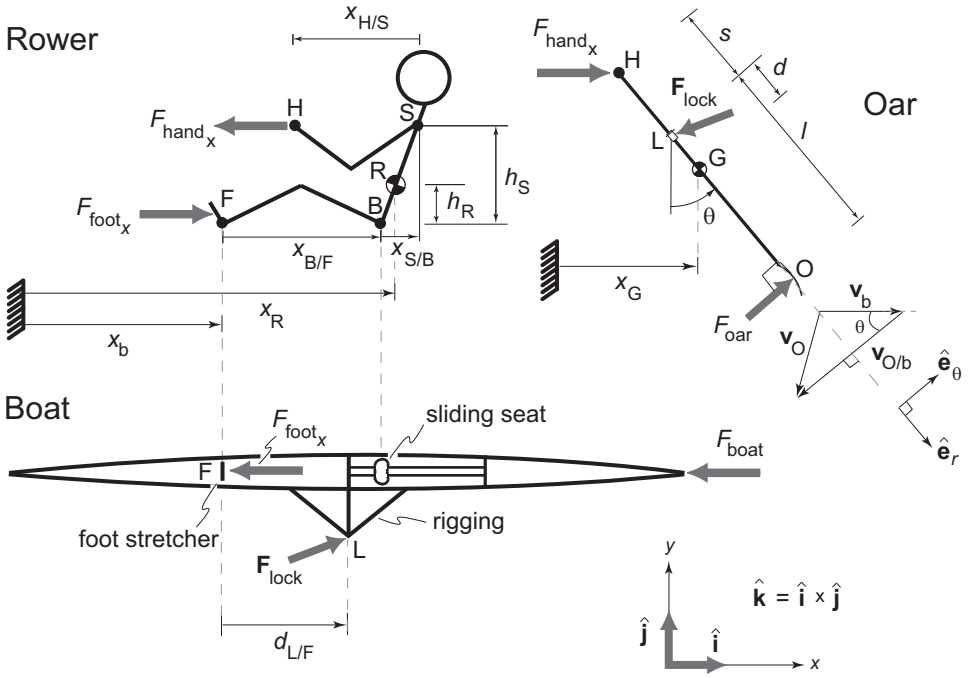

Fig. 1. **The model.** A geometric schematic and free body diagrams of the model used for both sculling and sweep rowing. Mass is located in the rower's gut, the oar, and the boat. Geometric constants are s, ℓ, d, h_{R}, h_{S}, and $d_{\mathrm{L/F}}$. Time-dependent geometric quantities are x_{R}, x_{b} $(= x_{\mathrm{F}})$, x_{O}, $x_{\mathrm{B/F}}$, $x_{\mathrm{S/B}}$, $x_{\mathrm{H/S}}$, θ, $\mathbf{v}_{\mathrm{b}}$, $\mathbf{v}_{\mathrm{O}}$, and $\mathbf{v}_{\mathrm{O/b}}$. $\mathbf{v}_{\mathrm{b}}$ is the boat velocity, $\mathbf{v}_{\mathrm{O}}$ is the oar blade velocity, and $\mathbf{v}_{\mathrm{O/b}}$ is the velocity of the blade with respect to the boat and is in the $\hat{\mathbf{e}}_\theta$-direction. See text for model details.

covery as $\dot{\theta} < 0$ and $\dot{\theta} > 0$, respectively.) Sculling can be modeled by changing geometric parameters and multiplying the oar force and mass by 2.

For the drive, linear momentum balance in the x-direction for the rower gives:

$$\begin{aligned} \sum F_x &= m_{\mathrm{R}}\ddot{x}_{\mathrm{R}}, \qquad \left(\ddot{x}_{\mathrm{R}} \equiv \frac{d^2 x_{\mathrm{R}}}{dt^2}\right) \\ -F_{\mathrm{hand}_x} + F_{\mathrm{foot}_x} &= m_{\mathrm{R}}\ddot{x}_{\mathrm{R}}, \end{aligned} \tag{1}$$

where $F_{\mathrm{hand}_x} = F_{\mathrm{hand}_\theta}\cos\theta$ is the component of the force at the oar handle in the x-direction, F_{foot_x} is the force at the foot stretcher in the x-direction, m_{R} is the rower's mass, and x_{R} is the absolute x-position of the rower's center of mass relative to the starting line.

Linear momentum balance in the x-direction for the boat gives:

$$\begin{aligned} \sum F_x &= m_{\mathrm{b}}\ddot{x}_{\mathrm{b}}, \\ -F_{\mathrm{boat}} - F_{\mathrm{foot}_x} + F_{\mathrm{lock}_x} &= m_{\mathrm{b}}\ddot{x}_{\mathrm{b}}, \end{aligned} \tag{2}$$

where F_{boat} is the magnitude of boat drag, F_{lock_x} is the force at the oarlock in the x-direction, m_{b} is the boat's mass, and x_{b} is the absolute x-position of the foot stretcher (fixed on the boat) relative to the starting line.

Linear momentum balance in the x-direction for the oar gives:

$$\begin{aligned} \sum F_x &= m_{\text{O}}\ddot{x}_{\text{O}}, \\ F_{\text{hand}_x} - F_{\text{lock}_x} + F_{\text{oar}_\theta}\cos\theta &= m_{\text{O}}\ddot{x}_{\text{O}}, \end{aligned} \tag{3}$$

where F_{oar_θ} is the $\hat{\mathbf{e}}_\theta$-component of the force at the oar blade, θ is the oar angle in a plane parallel to the water, m_{O} is the oar's mass, and x_{O} is the absolute x-position of the oar's center of mass relative to the starting line.

Finally, angular momentum balance for the oar about a non-accelerating point instantaneously conincident with the oarlock gives:

$$\begin{aligned} \left\{\sum \mathbf{M}_{/\text{L}}\right\}\cdot\mathbf{k} &= \left\{\dot{\mathbf{H}}_{/\text{L}}\right\}\cdot\mathbf{k}, \\ \left\{\mathbf{r}_{\text{H/L}}\times\mathbf{F}_{\text{hand}} + \mathbf{r}_{\text{O/L}}\times\mathbf{F}_{\text{oar}}\right\}\cdot\mathbf{k} &= \left\{\mathbf{r}_{\text{G/L}}\times m_{\text{O}}\mathbf{a}_{\text{G}} + I_{\text{G}}\ddot{\theta}\mathbf{k}\right\}\cdot\mathbf{k}, \\ -F_{\text{hand}_x}s\cos\theta + F_{\text{oar}_\theta}\ell &= m_{\text{O}}d\cos\theta\ddot{x}_{\text{b}} + (I_{\text{G}} + m_{\text{O}}d^2)\ddot{\theta}, \end{aligned} \tag{4}$$

where $\sum \mathbf{M}_{/\text{L}}$ are the moments about the oarlock due to the forces at the oar handle and oar blade, $\mathbf{H}_{/\text{L}}$ is the oar's angular momentum about the oarlock, $\mathbf{k}$ is the unit vector in the z-direction, $\mathbf{r}_{\text{H/L}}$ is the position of the rower's hands relative to the oarlock, $\mathbf{r}_{\text{O/L}}$ is the position of the oar blade relative to the oarlock, $\mathbf{r}_{\text{G/L}}$ is the position of the oar's center of mass relative to the oarlock, $\mathbf{a}_{\text{G}}$ is the absolute acceleration of the oar's center of mass, I_{G} is the polar moment of inertia of the oar about its center of mass, s is the inboard oar length, ℓ is the outboard oar length, and d is the distance from the oarlock to the oar's center of mass. We assume that the hand force is in the x-direction.

Rower and oar center of mass positions, x_{R} and x_{O}, are given by the kinematic relations:

$$\begin{aligned} x_{\text{R}} &= x_{\text{b}} + x_{\text{B/F}} + r x_{\text{S/B}}, \\ x_{\text{O}} &= x_{\text{b}} + d_{\text{L/F}} + d\sin\theta, \end{aligned} \tag{5}$$

where $x_{\text{B/F}}$ is the hip position with respect to the feet, $r = h_{\text{R}}/h_{\text{S}}$ is the ratio of rower center of mass height to shoulder height from the seat, $x_{\text{S/B}}$ is the shoulder position with respect to the hips, and $d_{\text{L/F}}$ is the fore-aft position of the oarlock with respect to the feet. Their accelerations are found by twice differentiating the positions with respect to time:

$$\ddot{x}_{\mathrm{R}} = \ddot{x}_{\mathrm{b}} + \ddot{x}_{\mathrm{B/F}} + r\ddot{x}_{\mathrm{S/B}}, \tag{6}$$

$$\ddot{x}_{\mathrm{O}} = \ddot{x}_{\mathrm{b}} + d\ddot{\theta}\cos\theta - d\dot{\theta}^2\sin\theta. \tag{7}$$

In our model, oar rotation is known once the rower's coordination and the oarlock fore-aft positioning are specified. Since the rower always has a grip on the oar handle, the fore-aft positions of the rower's hand and the oar handle relative to the foot stretcher are the same. So, we have:

$$d_{\mathrm{L/F}} - s\sin\theta = x_{\mathrm{B/F}} + x_{\mathrm{S/B}} - x_{\mathrm{H/S}}, \tag{8}$$

where the left and right hand sides are the oar handle and rower hand position with respect to the foot stretcher, respectively. The term $x_{\mathrm{H/S}}$ is the hand position with respect to the shoulders. Here, we are only considering the movement of the arm in the fore-aft direction even though the actual path of the hands relative to the boat nearly follows the arc of a circle. In effect, we are neglecting the projected arm shortening due to the arms not being parallel to the boat. Rewriting the above expression and differentiating twice with respect to time we get:

$$s\ddot{\theta}\cos\theta = \ddot{x}_{\mathrm{H/S}} - \ddot{x}_{\mathrm{B/F}} - \ddot{x}_{\mathrm{S/B}} + s\dot{\theta}^2\sin\theta. \tag{9}$$

For the recovery, the governing equations are the same as for the drive except that the force of the water on the oar blade is zero and that of the air is neglected.

2.3 Drag on the Boat

The drag force (D) on an object (e.g. oar or boat) moving at constant velocity in a stationary medium (or, equivalently, a stationary object in a constant far field velocity crossflow) is typically written as a function of fluid density (ρ), a characteristic area (A), and velocity (v). $D = (1/2)\rho CAv^2$ where (nondimensional) C is typically dependent on Reynolds number (ratio of inertial to viscous forces) as well as the object's shape (e.g., see Fox & McDonald (1992)). Drag tests performed by Hoerner (1965) and Wellicome (1967) further support this suggested quadratic relationship for rowing boats. Therefore, we use the following expression for boat drag in our model:

$$F_{\mathrm{boat}} = C_1\dot{x}_{\mathrm{b}}^2, \tag{10}$$

where $C_1 = (1/2)\rho CA$ is the boat drag coefficient. Fluctuations in boat velocity during a stroke are typically on the order of $\pm 25\%$ of the average velocity. So the Reynolds number, defined by $R_e = vL/\nu$ (where L is a characteristic

length and ν is the fluid's kinematic viscosity), does not vary much during the stroke. Therefore, C should mostly depend on boat shape. Furthermore, in his study of the relationship between boat speed and number of oarsman, McMahon (1971) noted that big and small boats have the same shape; the ratio of boat length to width is relatively constant for all boat types. Lazauskas (1998) also reports relatively constant ratios of boat length to width and boat length to depth for several boat types, further supporting this notion of geometric similarity. Based on these findings, one can take C to be roughly constant across all boat types. C_1 is then approximately just a function of the boat's characteristic area, A, which then varies with the square of boat length. A could be wetted area or the projected cross-sectional area. A more accurate value of C or C_1 could be determined for a given boat using drag data where the boat speed fluctuates rather than being pulled at a constant speed.

2.4 Models of the Oar Blade Force

We tried two different force-velocity relationships to model the oar-fluid interaction, finding F_{oar_θ} from the blade velocity, $\mathbf{v}_\mathrm{O} = v_\mathrm{b}\sin\theta\hat{\mathbf{e}}_r + (\ell\dot{\theta} + v_\mathrm{b}\cos\theta)\hat{\mathbf{e}}_\theta$.

Model 1 is that of Pope. Pope assumes that the resultant force is only in the $\hat{\mathbf{e}}_\theta$-direction and that the magnitude of the force is proportional to the square of the component of blade velocity in the $\hat{\mathbf{e}}_\theta$-direction:

$$F_{\mathrm{oar}_\theta} = C_2(\mathbf{v}_\mathrm{O}\cdot\hat{\mathbf{e}}_\theta)^2 = C_2(\ell\dot{\theta} + \dot{x}_\mathrm{b}\cos\theta)^2, \tag{11}$$

where $C_2 = (1/2)\rho C' A'$ is the equivalent blade force coefficient, A' is the area of the face of the oar blade, and C' is a shape-determined constant.

Model 2 of the oar blade force is based on the quasi-steady model used by Wang et al. (2004) for predicting the forces on a hovering insect wing. This model takes into account lift and drag forces on the blade, where drag opposes the blade velocity and lift is perpendicular to drag as depicted in Fig. 2. The magnitudes of the lift and drag forces, F_lift and F_drag, are proportional to the square of blade velocity, $\mathbf{v}_\mathrm{O}$:

$$F_\mathrm{lift} = C_L|\mathbf{v}_\mathrm{O}|^2, \tag{12}$$
$$F_\mathrm{drag} = C_D|\mathbf{v}_\mathrm{O}|^2, \tag{13}$$

where the lift and drag coefficients, C_L and C_D, are functions of the angle of attack, ϕ, the angle between the blade velocity relative to the fluid and the $\hat{\mathbf{e}}_r$-direction as shown in Fig. 2. The relationships between C_L, C_D, and ϕ are shown in the *lift-drag polar* (the plot of C_L versus C_D) in Fig. 2. In particular, we have:

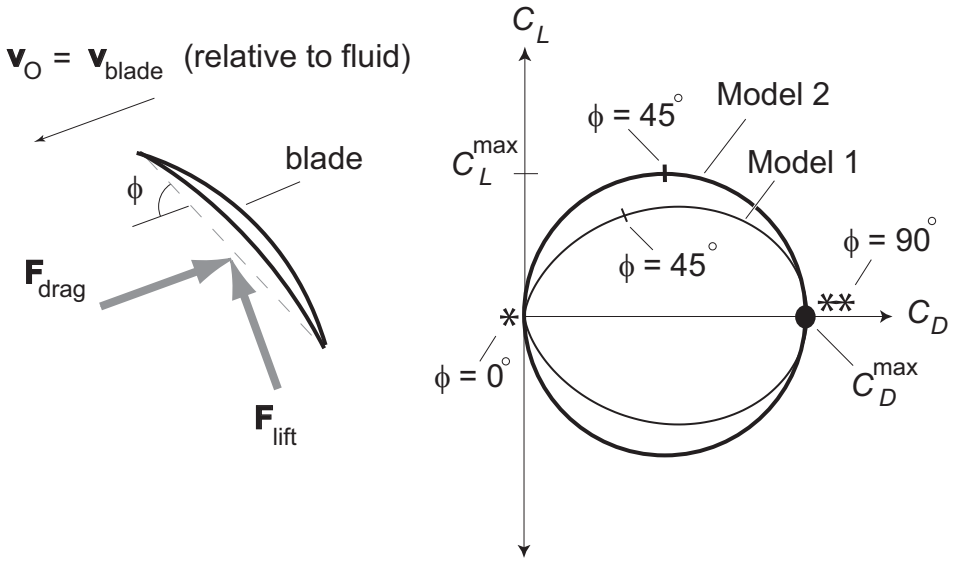

Fig. 2. **Oar force models.** In Model 2 of the oar blade force, the resultant fluid force on the oar blade is broken up into *lift* and *drag* as shown on the left. The angle of attack, ϕ, is the angle between $\mathbf{v}_{\text{blade}}$ and the axis of the plate. The relationship between the lift and drag coefficients is shown on the right for both models of the oar blade force. The equivalent lift and drag forces of Model 1 are the forces in Model 2 multiplied by $\sin\phi$. When $\phi = 0$ or 180° (marked with a $*$ in the plot of C_L versus C_D), there is no lift and the drag force is at a minimum (zero in this case as we neglect the thickness of the plate). When $\phi = 90°$ (marked with a $**$) the plate is perpendicular to the flow and the lift is zero but the drag now attains its maximum value. In aerodynamics, the region near $\phi = 0°$ $(*)$ is of central importance. In rowing, near $\phi = 90°$ $(**)$ is most relevant.

$$C_L = C_L^{\max} \sin 2\phi, \tag{14}$$
$$C_D = C_L^{\max}(1 - \cos 2\phi), \tag{15}$$

where $C_L^{\max}$ is the maximum lift coefficient. This force turns out to be orthogonal to the blade. In the end we found the model results from this model similar enough to those from Model 1 that we used Model 1 for most of our calculations.

2.5 Transition Rule at Catch and Finish

Rowers avoid splash at the *catch* (when the oars are put in the water). Too much backsplash is naturally considered bad and a late catch results in "missed water." We assume *a priori* that the rowers perfectly avoid backsplash and missed water. The drive starts when the velocity of the oar blade's absolute

velocity normal to the blade is zero, i.e.

$$\mathbf{v}_{\mathrm{O}} \cdot \hat{\mathbf{e}}_\theta = 0. \tag{16}$$

Note that the reaction force on a submerged blade is zero at the start of the drive for both models of the blade dynamics. In Model 1 we define the force as being proportional to the square of the normal velocity so the force will be zero at the catch. In Model 2, when there is no $\hat{\mathbf{e}}_\theta$ component to the blade velocity, the angle of attack is 0° and the lift and drag coefficients are both 0 (point $*$ in Fig. 2).

Rowers also avoid an early and a late *release* (when the oars are removed from the water). Finishing late results in a braking effect while finishing early results in missed water. Therefore, we end the drive when the force on the blade is exactly zero which, again, corresponds to $\mathbf{v}_{\mathrm{O}} \cdot \hat{\mathbf{e}}_\theta = 0$ in both oar models.

2.6 Model Summary

Equations 1–7, 9 and the boat and oar drag laws (Equations 10 and 11) completely define the state of the system of rower, boat, and oar. These equations are linear in the forces and accelerations. Therefore, at any time t we have a linear system of 7 equations in 10 unknowns. We can write this system in the following matrix form:

$$[A]\mathbf{z} = \mathbf{b}, \tag{17}$$

where

$$A = \begin{bmatrix} m_{\mathrm{r}} & 0 & 0 & 0\,0 & 0 & 0 & 1/\cos\theta & -1 & 0 \\ 0 & m_{\mathrm{b}} & 0 & 0\,0 & 0 & 0 & 0 & 1 & -1 \\ 0 & 0 & m_{\mathrm{O}} & 0\,0 & 0 & 0 & -1/\cos\theta & 0 & 1 \\ 0 & m_{\mathrm{O}} d\cos\theta & 0 & 0\,0 & 0 & I_L & s & 0 & 0 \\ -1 & 1 & 0 & 1\,r & 0 & 0 & 0 & 0 & 0 \\ 0 & 1 & -1 & 0\,0 & 0 & d\cos\theta & 0 & 0 & 0 \\ 0 & 0 & 0 & 1\,1 & -1 & s\cos\theta & 0 & 0 & 0 \end{bmatrix},$$

$$\mathbf{z} = \begin{bmatrix} \ddot{x}_{\mathrm{R}} & \ddot{x}_{\mathrm{b}} & \ddot{x}_{\mathrm{O}} & \ddot{x}_{\mathrm{B/F}} & \ddot{x}_{\mathrm{S/B}} & \ddot{x}_{\mathrm{H/S}} & \ddot{\theta} & F_{\mathrm{hand}_\theta} & F_{\mathrm{foot}_x} & F_{\mathrm{lock}_x} \end{bmatrix}^T,$$

$$\mathbf{b} = \begin{bmatrix} 0 & -F_{\mathrm{boat}} & F_{\mathrm{oar}_\theta} & \ell F_{\mathrm{oar}_\theta} & 0 & d\dot{\theta}^2\sin\theta & s\dot{\theta}^2\sin\theta \end{bmatrix}^T.$$

In order to solve the above system we generally need to know $10 - 7 = 3$ of the 10 forces and accelerations in $\mathbf{z}$. (Note: Specifying $x(t)$ implicitly specifies

$\ddot{x}(t)$.) Prescribing more than 3 variables leads to an overdetermined system and no solutions (unless the prescribed functions are perfect) while prescribing less than three variables leads to an underdetermined system and an infinite number of solutions. However, there are instances where nonunique solutions exist even when we specify 3 variables. Specifically, if none of the body positions ($x_{\mathrm{B/F}}$, $x_{\mathrm{S/B}}$, and $x_{\mathrm{H/S}}$) is one of the three specified variables, then any vector $[x_{\mathrm{B/F}},\ x_{\mathrm{S/B}},\ x_{\mathrm{H/S}}]$ that satisfies $[A]\mathbf{z} = \mathbf{b}$ can have any vector proportional to $[-r,\ 1,\ 1-r]$ added to it without affecting any other forces and accelerations. That is, the rank of A reduces from 7 to 6 if 3 columns are removed and none of the 3 are columns 4, 5, or 6. The reason for this redundancy is due to the fact that we use 3 variables ($x_{\mathrm{B/F}}$, $x_{\mathrm{S/B}}$, $x_{\mathrm{H/S}}$) to characterize 2 dynamic degrees of freedom ($x_{\mathrm{H/R}}$, $x_{\mathrm{R/F}}$). The extra body degree of freedom is left in for better comparison with data.

A common practice in the modelling of biomechanical tasks is to drive the model with muscle forces, joint torques, or muscle activation patterns (e.g. Atkinson). Instead, we drive our model by prescribing the rower's coordination ($x_{\mathrm{B/F}}$, $x_{\mathrm{S/B}}$, and $x_{\mathrm{H/S}}$) as functions of time (e.g. Alexander). In the end, the ability of the model to fit data does not depend on whether forces or motions are prescribed in the differential equation solutions.

Once the body positions are prescribed we also know their accelerations by twice differentiating the positions. Furthermore, the equations for boat drag and oar blade force (being dependent on velocity and not on acceleration) are uncoupled from the remaining equations. Thus, the system of governing equations reduces to 7 equations in 7 unknowns whose solution may be obtained at any time t by a matrix inversion. Thus, Equation 17 can be solved at each instant in time for use in a numerical ordinary differential equation (ODE) solver to find all variables as functions of time. For convenience, we further simplify the set of equations by combining them to eliminate all of the unknown forces (F_{hand_θ}, F_{foot_x}, F_{lock_x}) and the rower and oar center of mass accelerations ($\ddot{x}_{\mathrm{R}}$, $\ddot{x}_{\mathrm{O}}$). Furthermore, since we prescribe the body positions, θ and its derivatives are known at any time from Equation 8. Therefore, we are left with a single, second order ODE in boat position (or, equivalently, a first order ODE in boat velocity):

$$\ddot{x}_{\mathrm{b}} = \frac{-F_{\mathrm{drag}} + F_{\mathrm{oar}_\theta}\cos\theta - m_{\mathrm{R}}(\ddot{x}_{\mathrm{B/F}} + r\ddot{x}_{\mathrm{S/B}}) - m_{\mathrm{O}}d(\ddot{\theta}\cos\theta - \dot{\theta}^2\sin\theta)}{m_{\mathrm{R}} + m_{\mathrm{b}} + m_{\mathrm{O}}}, \quad (18)$$

where F_{drag} and F_{oar_θ} are quadratic in boat velocity, $\dot{x}_{\mathrm{b}}$. After solving this ODE we can determine all of the forces, accelerations, velocities, and positions needed to compare with documented data.

For each numerical integration the body coordination is given ($x_i(t)$ given). However, we allow the coordination to vary from one simulation to the next

Table 1
Listed are the values of the variables fixed in the simulations. The first value listed is for singles while the second is for fours. The resulting mass is divided by four for the simulation of fours.

Variable	Value	Description
T	1.94, 1.65 s	stroke period
m_{R}	75, 92 kg	rower mass
s^*	0.89, 1.16 m	actual inboard oar length
s	0.83, 1.01 m	modified inboard oar length ($s^* - 0.06$ m, sculls; $s^* - 0.15$ m, sweeps)
ℓ^*	2.02, 2.62 m	actual outboard oar length
ℓ	1.805, 2.36 m	modified outboard oar length (ℓ^*-(blade length)/2)
m_{O}	1.2, 2.6 kg	oar mass
m_{b}	19.7, 14.475 kg	boat mass
C_1	3.16, 1.99 N/(m/s)^2	boat drag coefficient ($F_{\mathrm{boat}} = C_1 v_{\mathrm{b}}^2$)
C_2	58.7, 84.5 N/(m/s)^2	oar drag coefficient ($F_{\mathrm{oar}_\theta} = C_2(\mathbf{v}_{\mathrm{O}} \cdot \hat{\mathbf{e}}_\theta)^2$)
r	0.4, 0.4	ratio of shoulder height to center of mass height ($h_{\mathrm{R}}/h_{\mathrm{S}}$)
d	0.565, 0.73 m	distance from oarlock to oar center of mass
I_{G}	0.85, 3.1 kg m^2	oar moment of inertia ($m_{\mathrm{O}}(\ell^* + s^*)^2/12$)

when we minimize errors between the model and on-water data.

2.7 Model Constants

Listed in Table 2.7 are the values of the model constants used in our simulations. The values of stroke period (T), rower mass (m_{R}), inboard oar length (s), outboard oar length (ℓ), and oar mass (m_{O}) are measured off of the water. The values of s are 6 cm and 15 cm less than the actual inboard oar lengths, s^*, assuming that the rower applies a force at the oar handle 6 cm and 15 cm from the end for sculls and sweeps, respectively. Also, ℓ is half of the blade length (21.5 cm for sculls, 26 cm for sweeps) less than the actual outboard oar length, ℓ^*. Boat mass, m_{b}, is the sum of the fully rigged boat mass and the mass of the data collection equipment. Boat added-mass is neglected because, using the relation $m_a/m_d = a/(3h - a)$ for a "Rankine ovoid" (taken as roughly the shape of a rowing shell) from Lighthill (1986) where m_a is the added mass, m_d is the displaced mass, a is boat width, and h is (roughly) boat length, the added mass is only 0.0065 of the displaced water mass. (Alexander assumed an overly large added mass of 0.2 of the displaced water mass.)

The boat drag coefficient, C_1, used in Equation 10 is computed as $C_1 = (1.07)(1/2)\rho C^* D^{2/3}$ where D is displaced volume (assuming $D^{2/3}$ is proportional to the boat's wetted area) and C^* is a nondimensional shape factor. The factor of 1.07, suggested by Pope, accounts for the additional (wave) drag

due to the deformation of the water surface. For eights we have drag test data that gives $C_1 = 11.8$ N/(m/s)^2 (from Lazauskas (1998)). We compute C_1 for fours and singles using geometric similarity, i.e. we take C^* as constant for all boat types. For fours, C_1 is divided by 4 since we only consider the motion of a single rower. Therefore, for fours we have $C_1 = (1.07)(11.8)/(4 \times 2^{2/3}) = 1.99$ N/(m/s)^2 and for singles we have $C_1 = (1.07)(11.8)/(8^{2/3})$ N/(m/s)^2 = 3.16 N/(m/s)^2.

The oar drag coefficient, C_2, is computed as $C_2 = (1/2)\rho C' A'$. The blade area, A', is 0.0903 m^2 for sculls and 0.13 m^2 for sweep oars (from measurements of the oar blades). The value of C' is obtained from a plot in Hoerner (1965) showing the drag coefficient as a function of Froude number, F_r, for a stationary flat plate perpendicular to a constant velocity crossflow. The plate is completely submerged but the top of edge of the plate is just below the free surface. The Froude number is computed as $F_r = V/\sqrt{gh}$ where V is the blade velocity, g is the acceleration of gravity, and h is the width of the blade. Using $V = 1$ m/s, $g = 9.81$ m/s^2, and $h = 25$ cm, we obtain $F_r \approx 0.64$ which corresponds to roughly $C' = 1.3$ from the Hoerner plot.

The ratio of rower center of mass height to shoulder height, r, is estimated from measurements of the masses and center of mass locations of a human (Zatsiorsky, 2002). Oar center of mass distance from the oarlock, d, and the oar's moment of inertia about its center of mass, I_G, are calculated assuming that the oar is a uniform rigid rod ($d = (\ell^* - s^*)/2$ and $I_G = m_O(\ell^* + s^*)^2/12$).

2.8 Model Analysis

2.8.1 Parameterization of the Body Position Functions

The method of parameterizing the body position functions is somewhat arbitrary. The only properties we require of the functions are that they be periodic (assuming that the rower reaches a steady-state) and twice differentiable (because we want continuous accelerations and forces). Periodic cubic splines satisfy both of these requirements and they also allow us to parameterize the curves using as many parameters as we desire. We have tried other parameterizations (Fourier Series, for example) and found the present choice adequate. The numerical procedure used to construct the splines is discussed in Appendix A.2.

2.8.2 Integration of the Governing Equations

The nonlinear ODE that governsboat position (Equation 18) cannot be solved analytically. Therefore, to integrate the equation we use a 4-stage, Runge-

Kutta method where the integration step size is held constant except near the spline knot times and near the transition times from recovery to drive and vice versa. In order to maintain the desired integration accuracy over the entire stroke period, we avoid integrating over the knot times (where the boat acceleration is nondifferentiable since the body accelerations are piecewise linear functions of time) by adjusting the integration step size so that we integrate to exactly these times. As a matter of convenience, the integration step size is chosen so that the integration times coincide exactly with the times at which the raw data is interpolated. Since the raw data we use is interpolated over fifty equal time intervals, we use an integration step size of $h = T/(2\times 50)$ where T is the stroke period. Using this step size and an arbitrary set of knot ordinates, convergence tests show that we are able to integrate boat velocity to within an absolute numerical error of 10^{-6} m/s. Transition times between drive and recovery are determined accurately by an iterative process outlined in Appendix A.3.

We seek steady-state motions of the rower-boat-oars system since the data collected is more-or-less periodic. Since the coordination is parameterized by periodic cubic splines, periodicity of the rower-boat-oars system will occur with the proper choice of boat velocity at the start of one stroke (see Appendix A.4).

2.8.3 Data Collection

The measurements were conducted during on-water rowing in a competitive single scull and four without coxswain (Jeff Sykes & Associates Pty Ltd.) The fully rigged boat masses were 15.8 and 52 kg, respectively, and Dreissigacker racing oars were used (CONCEPT2 Inc., Vermont, USA). See Appendix A.5 for detailed descriptions of the measurement techniques and data analysis.

Two data sets are used to validate the model:

(1) a set of women's singles; measured were 5 functions of time: $\tilde{x}_{\mathrm{B/F}}(t)$, $\tilde{x}_{\mathrm{S/B}}(t)$, $\theta(t)$, $F_{\mathrm{hand}_\theta}(t)$, and $\dot{x}_{\mathrm{b}}(t)$ and
(2) a set of men's fours (without coxswain); measured were 4 functions of time: $\tilde{x}_{\mathrm{B/F}}(t)$, $\theta(t)$, $F_{\mathrm{hand}_\theta}(t)$, and $\dot{x}_{\mathrm{b}}(t)$. We think of all derivatives and integrals of the measured quantities as measured data.

The functions $\tilde{x}_{\mathrm{B/F}}(t)$ and $\tilde{x}_{\mathrm{S/B}}(t)$ are the leg and back displacements from their positions at $t = 0$. That is, $\tilde{x}_{\mathrm{B/F}}(t) = x_{\mathrm{B/F}}(t) - x_{\mathrm{B/F}}(0)$ and $\tilde{x}_{\mathrm{S/B}}(t) = x_{\mathrm{S/B}}(t) - x_{\mathrm{S/B}}(0)$.

2.8.4 Measurement of Model vs. Data Error

We validate the model by showing how closely it can simulate the observed forces and motions observed. We quantify how well the simulated variables compare with the measured data using an analysis similar to that of McLean et al. (2003) wherein both kinematic and dynamic consistency between model and data is desired. The data collected have different scales and units and we have more data for singles than we do for fours. Therefore, we construct a measurement of error, J, between the model and on-water data that is unit-independent, reasonably scaled, and independent of the number of curves to be fitted. See Appendix A.6 for a detailed description of the function, J, used to quantify the net error. Appendix A.6 also describes how the coordination patterns (motions and, thus, through the governing equations, forces) are found.

2.9 Root Finding Versus Minimization

Minimizing the net error, J, may turn out to be a root finding problem (with $J = 0$ as a solution) depending on how many variables we fit. For clarification we define the following:

- n_f = number of functions of time in the model. We count $x(t)$, $\dot{x}(t)$, and $\ddot{x}(t)$ together as one function of time. For this model, $n_f = 10$ and the functions are listed in Equation 17.
- n_e = number of independent equations to solve. These include momentum balance and kinematic constraint equations (as well as drag laws). We do not count $v(t) = dx/dt$ and $a(t) = dv/dt$ as equations for any kinematic variable x. For this model, $n_e = 7$ and the equations are given by Equations 1–4, 6, 7, and 9.
- n_v = number of variables (functions of time) measured in each data set. For data set 1 we have $n_v = 4$ and for data set 2 we have $n_v = 5$.
- n_u = number of measured variables used to evaluate the ultimate error. We will always evaluate the ultimate error using all n_v measured variables so $n_u = n_v$.
- n_m = number of measured variables used in the evaluation of J, i.e. used in the minimization of model versus on-water data error. We do not necessarily use all data for assessment of J because we want to know what data predicts what other data so $n_m \leq n_u$.
- n_s = number of functions prescribed for the ODE solution. To obtain a unique, exact solution to the governing equations of our model, $n_s \equiv n_f - n_e = 10 - 7 = 3$. We always solve the ODE using $n_s = 3$. An alternative we don't use is to not solve the ODE explicitly and include the degree of ODE satisfaction as part of the error to be minimized in the curve fitting. Instead, we always solve the ODE exactly (to numerical precision) using

prescribed functions ($x_{\mathrm{B/F}}(t)$, $x_{\mathrm{S/B}}(t)$, $x_{\mathrm{H/S}}(t)$) whether or not we have data for these functions. In other words, periodic ODE solution is a (pre-satisfied) constraint in our error minimization problem.

Since we need to specify 3 forces and/or accelerations (or positions/velocities) in order to solve the governing equations (Equation 17) we can generally fit the data exactly if we fit no more than 3 data variables ($n_m \leq 3$) and we parameterize each input function with at least as many parameters, n, as we have data points, N. The J-minimizing solutions will be unique if we fit at least three variables ($n_m \geq 3$) and at least one of these variables is one of the three body position functions ($x_{\mathrm{B/F}}, x_{\mathrm{S/B}}, x_{\mathrm{H/S}}$). The latter condition is necessary due to the existence of a non-zero vector in the null space of the A-matrix in Equation 17 as mentioned earlier. If we fit more than 3 variables ($n_m > 3$) we cannot expect to drive J to zero no matter how many parameters we use to parameterize our input functions, unless the model and reality coincide exactly.

In all but one of our simulations we use $n < N$ so in these cases we will always have $J > 0$. Furthermore, we always fit at least three variables and one of these variables is always $\tilde{x}_{\mathrm{B/F}}$ so we always have a unique minimal-J solution.

3 Results

Plots of force and motion time histories from the best fit simulation of singles using $n_m = 5$ and $n = 16$ (see Appendix A.7 for a discussion of the choice of n) along with the measured data are shown in Fig. 3 for Model 1. Agreement with the measured data is apparent in both the shape and magnitude of the time histories. The contributions to the fit error, J, are shown in the first row of Table 2 (trial a). The largest error is due to differences in oar angle while the smallest error is in the prediction of back position. The averages of the magnitudes of the residuals, $R(\hat{Y}_j) = \sum_{j=1}^{N} |Y_{ij} - \hat{Y}_{ij}|/N$, are also shown in the first row of Table 2. Using both models of the oar blade force, the residuals are less than 2.1° for oar angle, 0.35 cm for seat slide, 0.13 m/s for boat velocity, 11 N for oar handle force, and 0.11 cm for back position.

The average residual magnitudes and the error contributions to J from the best fit simulation of fours using $n_m = 4$ and $n = 16$ are shown in the fourth row of Table 2 (trial d). Again, the largest error contribution is from differences in oar angle while the best fit variable is leg position. As in the simulation of singles, we also find good agreement for fours. The averages of the residual magnitudes in this case are less than 2.2°, 0.26 cm, 0.15 m/s, and 26 N for oar angle, seat slide, boat velocity, and oar handle force, respectively. Given the good agreement for both models, we use Model 1 in all subsequent simulations

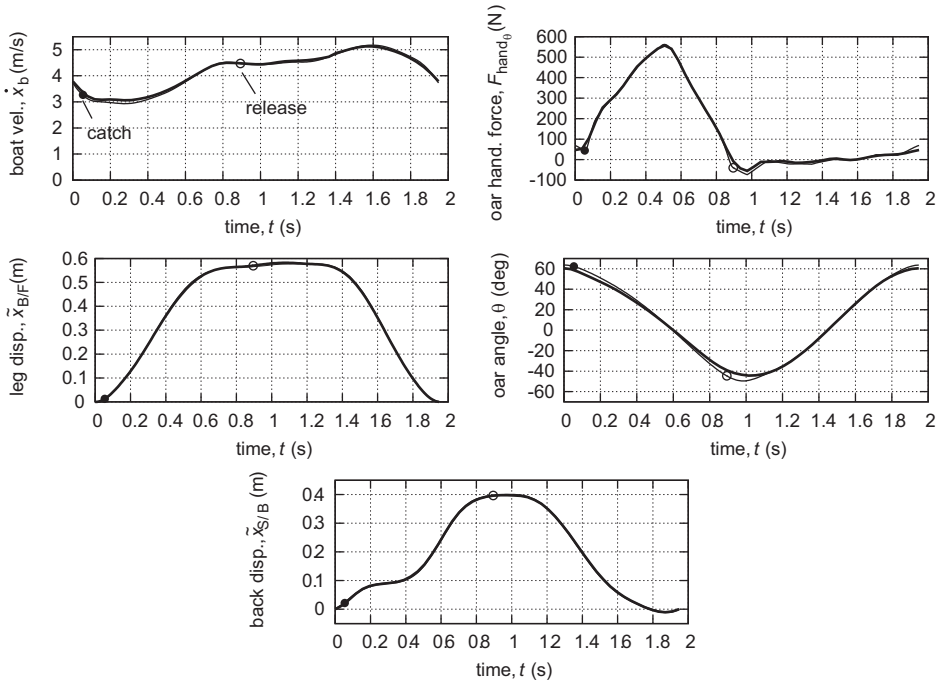

Fig. 3. **Best fit.** Comparison of the simulated and measured curves for the best fit simulation of singles where we fit all of the measured variables (see Table 2a). Here, we use Model 1 for the oar blade force and 16 parameters to define each coordination spline. The heavy, solid curves are the measured data while the thin, solid curves are the simulated results. The catch is indicated in each plot with a filled circle while the release is indicated with an open circle. Note that with a poor physical model we could only fit 3 of these curves at a time.

as it is conceptually simpler than Model 2.

4 Discussion

4.1 Predicting Unfit Variables

A measure of the model's ability to well simulate observed forces and motions is how well it can predict unfit variables. We test the model's ability to do this by (1) fitting for all variables except for boat velocity ($n_m = 4$ for singles, $n_m = 3$ for fours) and (2) fitting for $\tilde{x}_{\mathrm{B/F}}$, $\tilde{x}_{\mathrm{S/B}}$, and θ for singles ($n_m = 3$).

Fig. 4 shows the simulated and measured boat velocity resulting from fitting $\tilde{x}_{\mathrm{B/F}}$, θ, $\tilde{x}_{\mathrm{S/B}}$, and F_{hand_θ} for singles. The resulting errors are listed in the second row of Table 2 (trial b). We notice from the table that, compared with the case when we fit all measured variables, the fits to $\tilde{x}_{\mathrm{B/F}}$, θ, $\tilde{x}_{\mathrm{S/B}}$, and F_{hand_θ} are slightly better while the error contribution due to differences in

Table 2
Listed are the errors, $R(\hat{Y}_j)$ and $E(\hat{Y}_j)$, in the prediction of the measured variables, $\hat{Y}_j$, for all minimizations performed to validate the model. $R(\hat{Y}_j)$ is the average residual magnitude and $E(\hat{Y}_j)$ is the error contribution to J for variable $\hat{Y}_j$ (see Appendix A.6). The penultimate column indicates which variables are fitted in each minimization. The ultimate error is the weighted sum of the errors, $E(\hat{Y}_j)$, divided by the number of measured variables. (Note: * is the error when a penalty is added for roughness in the leg and back position curves.)

trial	data set	$\hat{Y}_j$	$R(\hat{Y}_j)$	$E(\hat{Y}_j)$	fitted?	ultimate error
a	1	$\dot{x}_{\mathrm{b}}$	0.053048 m/s	0.00023121	fit	0.00024192
		$\tilde{x}_{\mathrm{B/F}}$	0.003162 m	0.00004363	fit	
		θ	2.01887 deg	0.00065243	fit	
		F_{hand_θ}	6.43392 N	0.00027439	fit	
		$\tilde{x}_{\mathrm{S/B}}$	0.000925 m	0.00000797	fit	
b	1	$\dot{x}_{\mathrm{b}}$	0.079532 m/s	0.00050840	predicted	0.00027935
		$\tilde{x}_{\mathrm{B/F}}$	0.001194 m	0.00000932	fit	
		θ	1.87307 deg	0.00055312	fit	
		F_{hand_θ}	7.76152 N	0.00032128	fit	
		$\tilde{x}_{\mathrm{S/B}}$	0.000600 m	0.00000462	fit	
c	1	$\dot{x}_{\mathrm{b}}$	0.392070 m/s	0.00904122	predicted	0.00353617
		$\tilde{x}_{\mathrm{B/F}}$	0.000451 m	0.00000127	fit	
		θ	0.099239 deg	0.00000138	fit	
		F_{hand_θ}	36.0826 N	0.00865295	predicted	
		$\tilde{x}_{\mathrm{S/B}}$	0.000580 m	0.00000407	fit	
d	2	$\dot{x}_{\mathrm{b}}$	0.145617 m/s	0.00072300	fit	0.00096626
		$\tilde{x}_{\mathrm{B/F}}$	0.002577 m	0.00003078	fit	
		θ	2.18270 deg	0.00101337	fit	
		F_{hand_θ}	25.5341 N	0.00213842	fit	
e	2	$\dot{x}_{\mathrm{b}}$	1.74873 m/s	0.04726161	predicted	0.02284396
		$\tilde{x}_{\mathrm{B/F}}$	0.002577 m	0.00003112	fit	
		θ	0.552746 deg	0.00006355	fit	
		F_{hand_θ}	17.9031 N	0.00148194	fit	
f	2	$\dot{x}_{\mathrm{b}}$	0.361990 m/s	0.00439295	predicted	0.0038239*
		$\tilde{x}_{\mathrm{B/F}}$	0.012922 m	0.00059961	fit	
		θ	1.90408 deg	0.00069936	fit	
		F_{hand_θ}	23.9773 N	0.00196224	fit	

boat velocity more than doubles. Despite the increased error in the prediction of boat velocity, the average of the residual magnitudes are still small ($\approx$ 0.08 m/s $\Rightarrow\approx$ 2%). In fact, the differences between the predicted velocities for these cases are almost indistinguishable (compare the predicted velocity curves in Figs. 3 ($n_m = 5$) and 4 ($n_m = 4$)).

The results after fitting $\tilde{x}_{\mathrm{B/F}}$, θ, and F_{hand_θ} for fours are listed in the fifth row of Table 2 (trial e). As explained in Section 2.9, the fits to $\tilde{x}_{\mathrm{B/F}}$, θ, and F_{hand_θ} are good, with the fit to θ being much better than that obtained when we fit all measured variables. However, the boat velocity is predicted rather poorly.

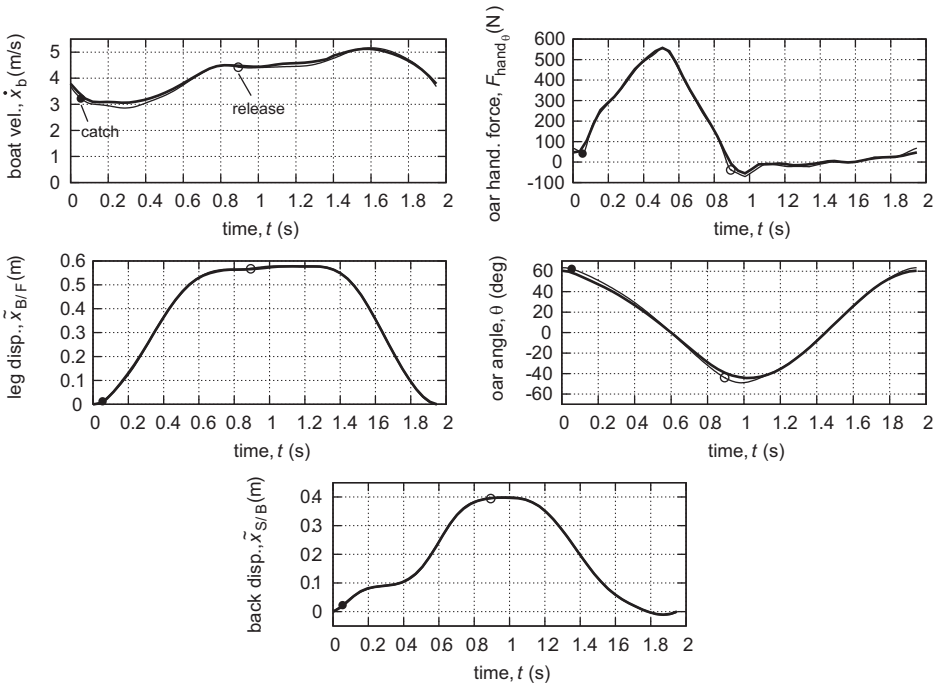

Fig. 4. **Predicting boat velocity.** Comparison of simulated (thin curves) and measured (heavy curves) results from the best fit simulation of singles where we fit F_{hand_θ}, $\tilde{x}_{\text{B/F}}$, θ, and $\tilde{x}_{\text{S/B}}$ ($n_m = 4$) (see Table 2b; boat velocity is *predicted*, not used in the fit). Here we see slightly less agreement with boat velocity than in the case when we fit for all variables. Nevertheless, the agreement is still good even though we don't fit for boat velocity and we don't reward smoothness in the body positions.

The predicted back velocity and acceleration curves contain several oscillations which contribute greatly to the poor prediction of boat velocity. The seat slide velocity and accelerations curves also contain oscillations, although they are not as pronounced as those in the back kinematic profiles. To get rid of these oscillations we added a penalty for non-smooth curves by minimzing J^* (see Appendix A.6). The model now does a reasonable job of predicting boat velocity (see plots in Cabrera (2005)). However, the predicted average boat velocity differs from the measured average velocity by about 0.37 m/s ($\approx$ 5% of 5.90 m/s). This discrepancy is most likely due to our choices of model constants, in particular, the oar drag coefficient and assumed location of the resultant blade force. Our predictions of all other variables are slightly worse as a result of penalizing roughness.

Another test of the model is to fit only three variables for singles and to see how well the model can predict the remaining measured variables. The resulting errors after fitting $\tilde{x}_{\text{B/F}}$, θ, and $\tilde{x}_{\text{S/B}}$ for singles (and trying to predict boat velocity and hand force) are shown in the third row of Table 2 (trial c). The largest error contribution is from differences in F_{hand_θ}. This error represents deficiencies in our model or parameter values. The shape of the velocity curve

matches the measured curve well but the simulated average speed is less than the measured average speed (3.83 m/s compared to 4.18 m/s). The peak oar handle force and the magnitude of the force during the recovery are matched well by the model but the shape and magnitude of the time histories during the drive do not agree well.

4.2 Fitting False Data

If the fits we obtain are a result of good curve fitting (as opposed to good modelling) then we should be able to obtain good fits to false data. We test the model in this manner by adding a sine wave to the boat velocity data for singles and finding best fits to this corrupted data for various amplitudes of the sine wave. Fig. 5a shows the value of $J_{\min}$ versus the amplitude of the corrupting sine wave. In general, perturbations to the velocity data decrease the quality of fit. We see in Fig. 5b that the minimization ignores the corrupted velocity (despite the penalty for lack of fit) and captures the original uncorrupted velocity. These results suggest that the fits we obtain are not the result of performing good curve fitting but rather the result of having a good model.

4.3 Sensitivity Analysis: How the fit depends on mechanical constants

Some model parameters (Table 2.7) are estimated since they were not measured when the force and kinematic measurements were taken. These estimates seem to be reasonable as we observe good agreement between simulation and measurements. However, it is possible that even better agreement may be achieved if we use different and, perhaps, more accurate values for these parameters. Fig. 6 shows plots of net error, $J_{\min}$, versus select model parameters for the simulation of singles. A single point on any one of these plots is generated by minimizing J, letting the rower's coordination and the oarlock fore-aft positioning be variable while fixing all other parameters to their values as listed in Table 2.7, except for the parameter indicated on the horizontal axis in each plot. The value of this parameter is held fixed during the minimization but is different from its nominal value. The filled circles in each plot correspond to the value of $J_{\min}$ when using the parameter listed in Table 2.7. The choices of C_1, r, and m_{b} appear to be nearly optimal. If we do not account for wave drag (i.e. we take out the factor of 1.07 when calculating C_1), the boat drag coefficient reduces to $C_1 = 2.95$ N/(m/s)^2 and we obtain slightly worse fits to oar handle force and oar angle. So it seems that accounting for wave drag is somewhat important.

We can achieve a slightly better fit if we choose $m_{\mathrm{b}} = 24$ kg (instead of 19.7 kg). This change corresponds to a boat added-mass of 4.3 kg which is

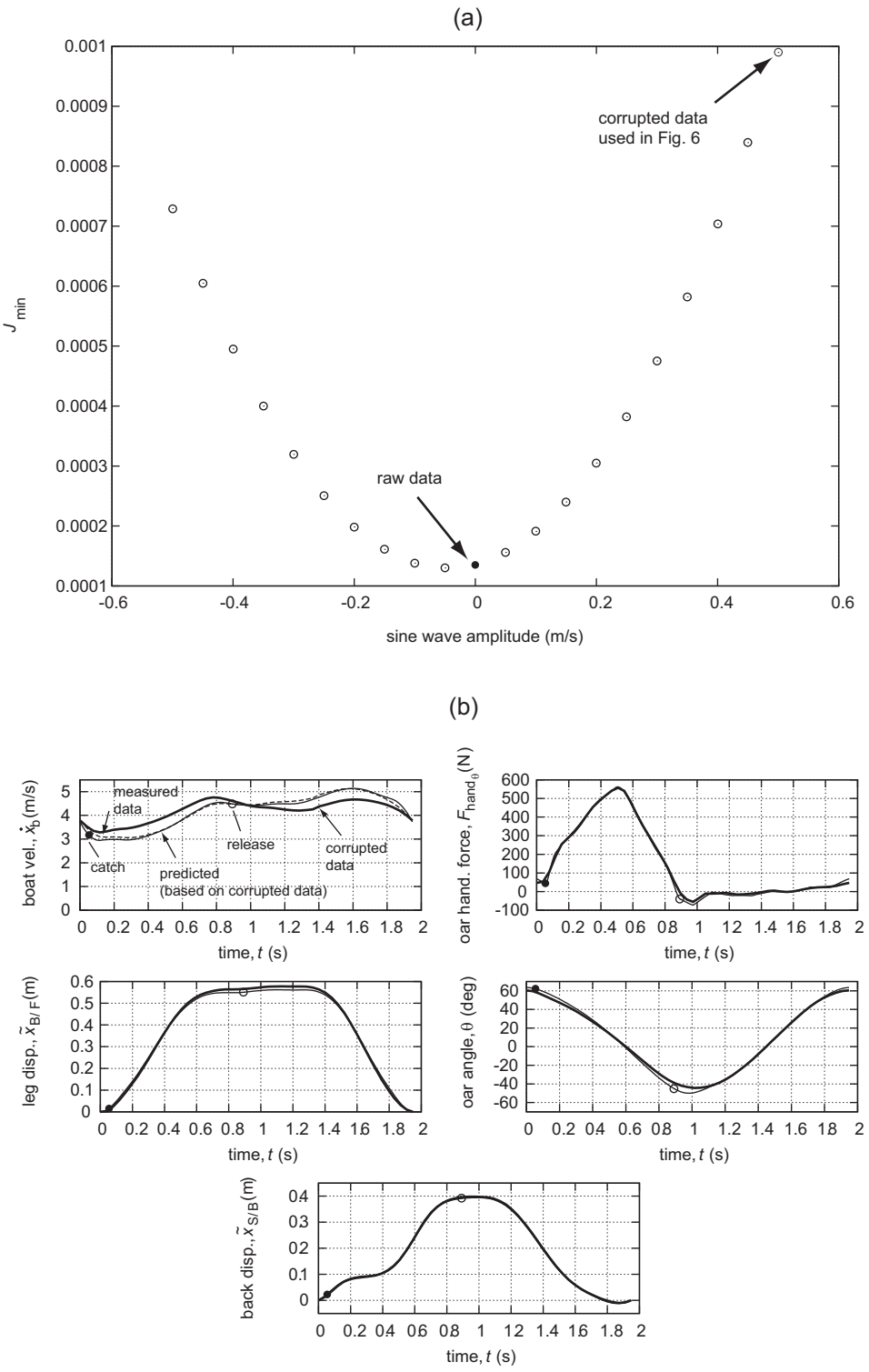

Fig. 5. **Fitting corrupted data.** (a) Plot of error, $J_{\min}$, versus the amplitude of the sine wave corrupting the boat velocity data for singles. The filled circle is the fit to the uncorrupted data. (b) Comparison of simulated (thin curves) and measured (heavy curves) results from the best fit simulation of singles where we fit all measured variables while corrupting the boat velocity data by the addition of the term: $0.50\sin(2\pi t/T)$ m/s. The dashed curve in the velocity plot is the original uncorrupted data. Note how the minimization essentially ignores the corruption term.

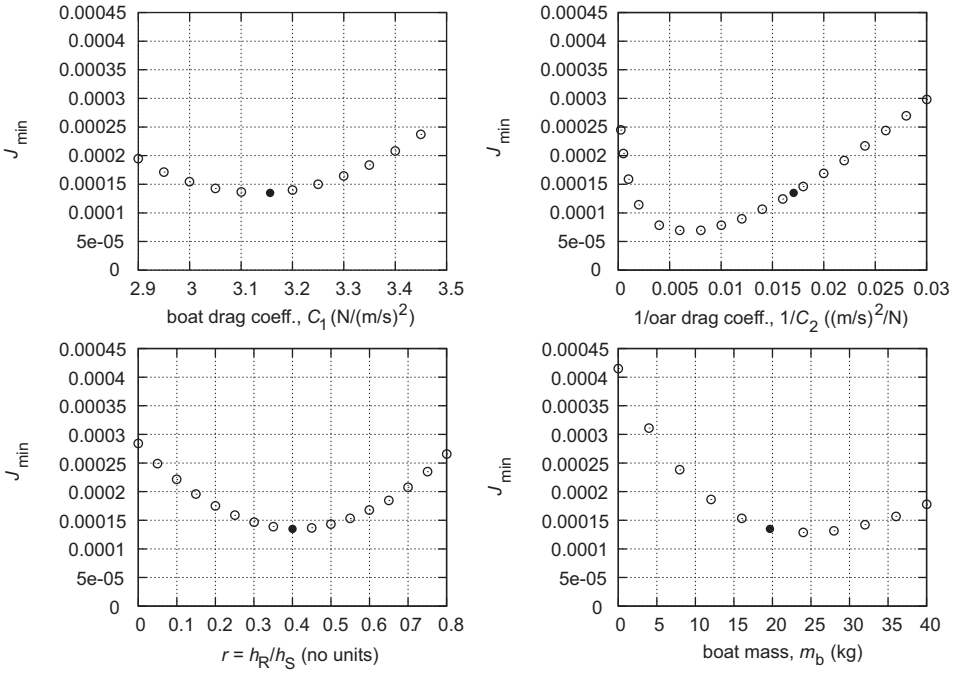

Fig. 6. Plots of $J_{\min}$ versus a single parameter value as the parameter is varied about the nominal values shown in Table 2.7. The filled circles correspond to the value of $J_{\min}$ at the nominal parameter values.

about 4.3% of the displaced mass but, still, a small percentage. Alternatively, instead of considering boat added-mass being due to fluid effects, we can think of it as being a fraction of the rower's mass put into the boat rather than into the rower's gut (not all of the rower's mass moves with the gut; for example, the rower's feet are attached to the boat and, thus, should probably be considered part of the boat). Taking 3.25 kg ($\approx 35\%$ of the foot and calf mass) of the rower's mass and putting it into the boat gives us a slightly better fit ($J_{\min} = 0.0002323654$).

However, the value of C_2 which minimizes the net error is about 2.4 times the nominal value we used. Using this near-optimal value of C_2, the best fit simulation results in a better prediction of oar angle ($E(\theta)$ is halved). Fig. 7 shows the path of the oar blade tip for three cases: (1) using the measured data, (2) using the nominal value of C_2, and (3) using a value of C_2 that is 2.4 times the nominal value. Using a larger C_2, we see that the model does a better job of predicting the actual path of the blade tip. Wang (2005) notes that during the transient motion of a plate accelerated from rest to a constant velocity, the maximum lift force is about 50% greater than the average lift force during steady-state. This suggests that larger values for C_2 and $C_L^{\max}$ should be used in our model. However, it is not certain that the lack-of-fit of the oar angle is necessarily due to a poor choice of C_2. The fact that the deviations between the predicted and measured angle are greatest near the catch and release indicate that perhaps our enforcement of the instantaneous transition

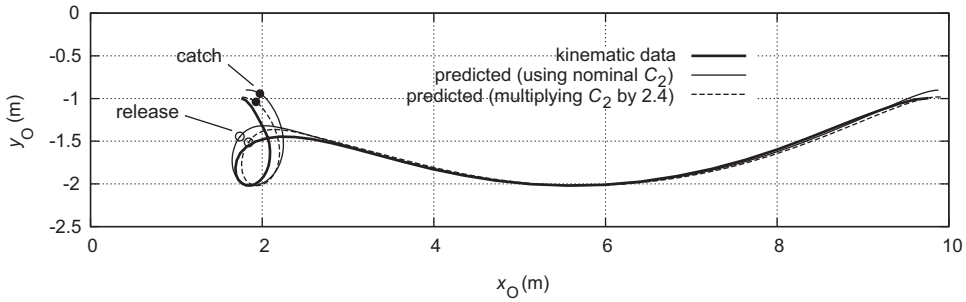

Fig. 7. Shown are traces of the tip of the oar blade (as viewed from above the water surface) (1) as indirectly inferred from boat velocity and oar angle data for singles (indicated by the heavy, solid line), (2) from the best fit simulation of singles using the oar drag coefficient in Table 2.7 (indicated by the thin, solid line), and (3) from the best fit simulation of singles using an oar drag coefficient 2.4 times the value of that in Table 2.7 (indicated by the dashed line).

from drive to recovery (and vice versa) when the blade normal velocity is zero is imperfect.

4.4 Unnecessary Improvements and Destructive Simplifications

4.4.1 Use $C_D = \infty$?

If the blade did not slip during the drive, it would cut through the water (following a tractrix) so that its velocity has a component only in the $\hat{\mathbf{e}}_r$-direction (see Fig. 1). Since the $\hat{\mathbf{e}}_\theta$-component of the blade velocity would be zero, we would have $\mathbf{v}_\mathrm{O} \cdot \hat{\mathbf{e}}_\theta = \ell\dot{\theta} + \dot{x}_\mathrm{b}\cos\theta = 0$. Differentiating this equation with respect to time gives us the following expression for the boat's acceleration, $\ddot{x}_\mathrm{b}$:

$$\ddot{x}_\mathrm{b} = \frac{\dot{x}_\mathrm{b}\dot{\theta}\sin\theta - \ell\ddot{\theta}}{\cos\theta}. \tag{19}$$

This would be equivalent to setting $C_D = \infty$ for the oar blade. So, enforcing the no-slip condition leads to the boat's motion being determined by the kinematics of the oar rather than the oar blade force, boat drag, or any masses. We determine the best fit to the singles data while enforcing the no-slip condition to determine whether or not the simplification produces similar results as the case when we allow for slip. The resulting best fit to all of the data ($n_m = 5$) for singles is shown in Fig. 8. The force applied at the oar handle is predicted rather poorly during the drive phase even though the remaining variables are well-predicted throughout the stroke. The predicted peak force applied at the oar handle is nearly twice that of the maximum measured force and there is a marked rise and fall of the force during the initial moments of the drive that is

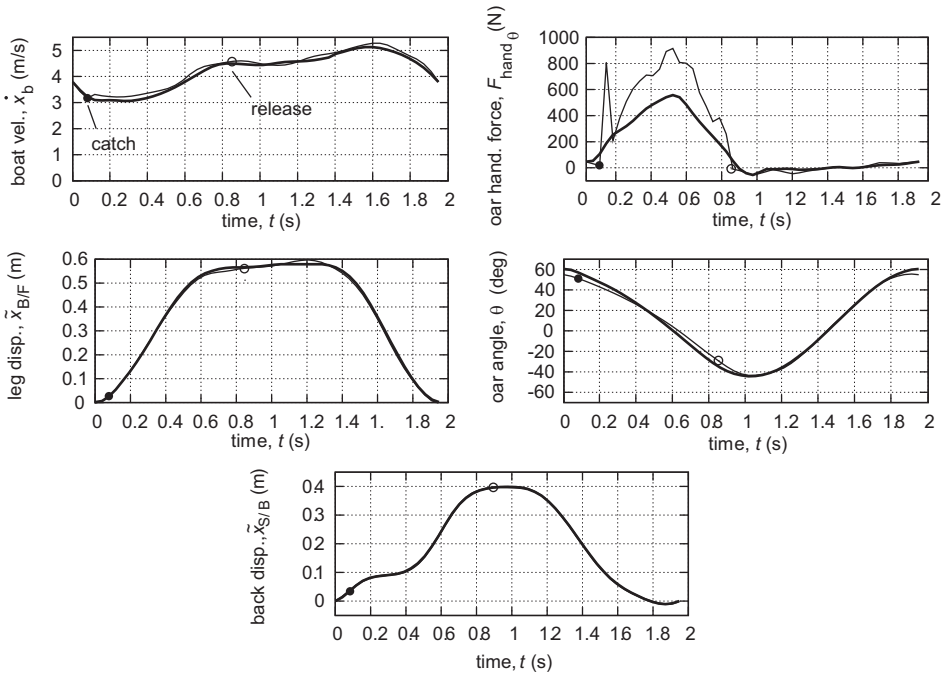

Fig. 8. Comparison of the simulated (thin curves) and measured (heavy curves) results from the best fit simulation of singles while enforcing no-slip of the oar blade. The oar handle force is poorly predicted in this case while the remaining variables are still well-predicted.

not seen in practice. Thus, the no-oar-slip simplification would prove to have a high cost in terms of model error.

4.4.2 Allowing for Oar Flexibility

In our model we assume a rigid oar. However, a study performed by Brearley & de Mestre (1998) shows that oars may bend anywhere from 2 to 7 degrees during on-water rowing, depending on oar type (sculls/sweeps) and stroke rate. We investigate the possible improvement of our model (better fits) by allowing for oar flexibility. We assume the oar is composed of two rigid rods (the inboard and outboard) with inertia, hinged together at the hinge with a torsional spring. The moment, M, applied to each rod by the spring is modelled as $M = K\Delta\theta$ where K is a constant and $\Delta\theta$ is the relative angle between the inboard and outboard. Due to the additional degree of freedom (the relative angle), there is an additional governing equation which is derived by taking angular momentum balance for the outboard portion of the oar about the oarlock. This gives us an equation for the relative angular acceleration of the two rods, $\Delta\ddot{\theta}$. Since the spring constant, K, is not known, it is included as a variable parameter. Fig. 9 shows the resulting best fits to all of the data for singles using $n = 16$. The value of the minimized cost function is $J_{\min} = 0.00038239$ and the error contributions to J are $E(\dot{x}_b) = 0.00004755$, $E(F_{\text{hand}_\theta}) = 0.00009349$,

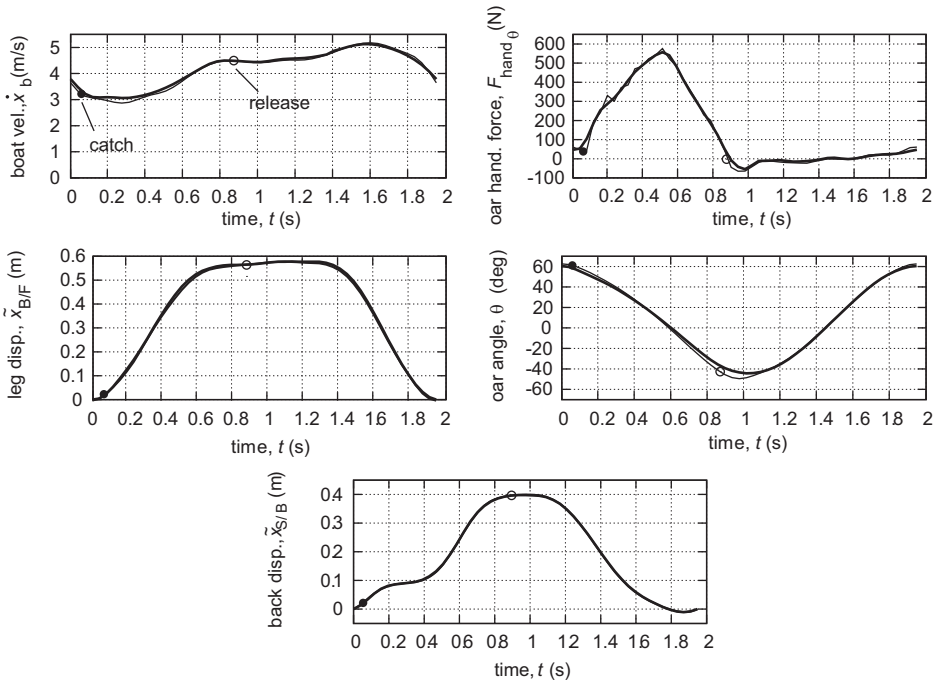

Fig. 9. Comparison of simulated and measured results from the best fit simulation of singles while accounting for oar flexibility. The addition of this flexibility does not improve the overall fit to the data so we deem this added improvement unnecessary.

$E(\tilde{x}_{\mathrm{B/F}}) = 0.00000730$, $E(\theta) = 0.00006123$, and $E(\tilde{x}_{\mathrm{S/B}}) = 0.00000160$. Comparing these errors with those of the best fit simulation using a stiff oar (Table 2a) we conclude that the addition of oar flexibility is an unnecessary improvement for fitting purposes.

4.5 Kinematic Complexity

One of the major simplifications is the pair of assumptions that (a) the resultant oar handle force is parallel to the boat and (b) the arms are parallel to the boat. Observation of real rowers shows this to be a drastic (perhaps over-) simplification. However, introducing force and motion of the arms not parallel to the boat would require more new assumptions than we thought would be useful.

5 Conclusion

We have constructed a model of rowing that does a reasonable job of imitating the forces and kinematics observed in actual rowing through comparison with documented data. The model accurately reproduces these forces and motions,

even those not included in the fit. Allowing oar slip proves to be necessary for accurately predicting the force generated at the oar handle. Allowing for oar flexibility, while making the model more realistic, does not result in better predictions.

The model seems promising for various rowing investigations such as: (1) using optimization to predict the coordination patterns that maximize boat speed subject to various biological constraints, (2) to determine the broadness of coordination and other system variables near an optimum to see what additional ingredients must be included in our optimization problem to predict the stereotypical legs-back-arms coordination pattern in rowing, and (3) to determine rigging changes for a boat with differently sized rowers or how coxswain motions might make a boat go faster.

Acknowledgements

The authors would like to thank William Atkinson and Leo Lazauskas for their helpful comments.

A Appendices

A.1 Previous Rowing Models

Recent rowing models that resemble Alexander's are those of Pope (1973), van Holst (2004), and Atkinson (2004). All of these models assume 1D momentum balance (yet account for large oar angles) and quadratic force-velocity relationships to model boat drag. To model the oar blade force, Pope uses Alexander's model which only considers drag while van Holst and Atkinson consider both lift and drag forces on the blade. The lift and drag forces are assumed to be proportional to the square of velocity, $F = Cv^2$, where v is the absolute blade velocity and C is the lift/drag coefficient which is a function of water density, blade surface area, and the angle of attack, i.e. the angle between the blade velocity and the oar longitudinal axis. Both van Holst and Atkinson consider boat added-mass as well as the oar's inertia in their models. Atkinson's model also accounts for oar flexibility, blade cant angle (angle between the oar shaft and the blade), and variation of the boat drag coefficient with water temperature and Reynolds number.

Like Alexander, Atkinson prescribes velocities of the rower's legs, back, and arms relative to the boat. However, Atkinson prescribes the force applied by the rower perpendicular to the oar handle as a function of time whereas

Alexander prescribes oar angle. Because, ultimately, both force and kinematic data are used in model fits, the difference between kinematic control (Alexander) and force control (Atkinson) is a matter of researcher taste, numerical convenience, and so on. In Pope's model, oar angular velocity and rower center of mass velocity relative to the boat are the dynamic degrees of freedom. Pope assumes that oar angular velocity is linearly proportional to the rower's center of mass velocity relative to the boat. He also assumes a constant instantaneous "propulsive efficiency" which he defines as the ratio of the rate at which "useful" work is done at the oar blade (the component of force at the oar blade in the direction of boat motion times boat velocity) to the power supplied by the rower at the oar handle. This second energetic assumption results in another kinematic coupling between oar angular velocity and rower velocity relative to the boat which then allows for the (numerical) solution of the boat's equation of motion. Van Holst prescribes both the component of the oar blade force in the direction of boat motion and the rower's center of mass position as functions of oar angle.

The above models are relatively simple and mechanically complete. Atkinson's and van Holst's models are more complex than the others in that they incorporate a slightly more complicated oar blade force law, requiring a look-up table or mathematical relationship to determine the lift and drag coefficients once the angle of attack has been calculated. These models require an iterative procedure to determine the oar angle once the blade force (in van Holst's model) or the force at the oar handle (in Atkinson's model) is specified. Also, in Atkinson's model, it is unknown whether oar flexibility, cant angle, and Reynolds number and temperature-dependent boat drag coefficient are necessary model ingredients. Although these models are mostly simple, none of them has been shown to accurately predict the forces and motions observed in actual rowing (with the exception of Atkinson who is able to accurately predict boat velocity). Alexander was presumably limited by the lack of data and computational power. Pope's model, while simple and easy to implement on a computer, is too simple to accurately model actual rowing. Instead of allowing his dynamic degrees of freedom (rower position relative to the boat and oar angle) to be freely selected, Pope assumes (but does not justify) a linear coupling between the two and provides another coupling based on his (flawed) measure of efficiency. Furthermore, due to his fixed duty cycle (ratio of the time when the oar is in the water to the period of the stroke), his model necessarily results in an (unrealistic) infinite acceleration and deceleration of the boat at the moments when the oar is inserted into and removed from the water, respectively. Atkinson's and van Holst's models, even with documented data to compare with, are limited in their predictive capabilities by the assumed forms of their dynamic degrees of freedom (force and rower velocity relative to the boat). Because no quantitative comparisons were made with measured variables (other than boat velocity in Atkinson's study), it is not known whether any of the assumptions used in the above models prevent the

models from accurately predicting the forces and motions experienced in an actual boat.

Our group at Cornell (Cardhana, Santos, Mukherjee, and Ruina (unpublished)) also posed several models in the spirit of Alexander's. However, until now, no results were objectively compared with on-water data, so no conclusions were reached about the veracity of the various assumptions.

Other simpler models posed by Sanderson & Martindale (1986), Millward (1987), Brearley & de Mestre (1996), Lazauskas (1997), and Simeoni et al. (2002) were developed to predict race times for various boat types. These models assume force and/or kinematic profiles that differ in many respects from those observed in real rowing. For example, Millward assumes that the force at the oarlock in the direction of boat motion has the shape of the square of a sine curve as a function of time and that this force acts for exactly half of the stroke period. None of these models is useful towards predicting forces and motions experienced during actual rowing. However, these models show that modelling the boat and rowers together as a single point mass can reasonably predict race times based on measured oar forces. That is, balancing average oar propulsive force with boat drag, based on average boat speed, gives reasonable predictions for average boat speed.

A.2 Constructing the Body Position Splines

We construct a spline by first selecting a set of points (t_i, x_i) (where $i = 1, \ldots, n+1$), called *knots*, through which we want the curve, $x(t)$, to pass. For convenience, we space the knots evenly in time starting at $t_1 = 0$ and ending at $t_{n+1} = T$ where $t_{i+1} = t_i + \Delta t = t_i + T/n$ for $i = 1, \ldots, n$. By spacing the knots evenly, our freedom in manipulating the spline is restricted to choosing only the knot ordinates, x_i, rather than both the ordinates, x_i, and the abscissae, t_i. We then construct a cubic function, $y_i(t)$, over each time interval $[t_i, t_{i+1}]$ for $i = 1, \ldots, n$. The cubic functions are given by $y_i(t) = A_i t^3 + B_i t^2 + C_i t + D_i$ where the constants A_i, B_i, C_i, and D_i are to be determined from the points (t_i, x_i) for $i = 1, \ldots, n$. Since each cubic, $y_i(t)$, is defined by 4 coefficients (A_i, B_i, C_i, D_i), and there are n cubic functions, we must determine a total of $4n$ constants to completely define the spline which is a concatenation of the n cubics. The constants are determined by satisfying the following $4n$ conditions:

- Each cubic passes through its endpoints: $y_i(t_i) = x_i$ and $y_i(t_{i+1}) = x_{i+1}$ for $i = 1, ..., n \Rightarrow 2n$ conditions.
- Adjacent cubics maintain continuity in their first and second derivatives at their points of intersection: $\dot{y}_{i-1}(t_i) = \dot{y}_i(t_i)$ and $\ddot{y}_{i-1}(t_i) = \ddot{y}_i(t_i)$ for $i = 2, ...n \Rightarrow 2n - 2$ conditions.

- To enforce periodicity, the first and last cubics maintain continuity in their first and second derivatives at $t = 0$ and $t = T$, respectively: $\dot{y}_1(t_1) = \dot{y}_n(t_{n+1})$, and $\ddot{y}_1(t_1) = \ddot{y}_n(t_{n+1}) \Rightarrow 2$ conditions.

The above $4n$ conditions result in a linear system of $4n$ equations with $4n$ unknown spline coefficients which are found with a standard linear solver.

A.3 Procedure for Determining the Recovery-to-Drive and Drive-to-Recovery Transition Times

We enforce the transition from recovery to drive (and vice versa) to occur when the slip velocity goes to zero (see Equation 16). The time when this transition occurs is calculated using an iterative procedure. Let τ_i be the time when the sign of the slip velocity changes and let v_{slip_i} be the slip velocity at this time. Then, using $(\tau_i, v_{\text{slip}_i})$ and the two integration times and slip velocities prior to the sign change ($(\tau_{i-1}, v_{\text{slip}_{i-1}})$ and $(\tau_{i-2}, v_{\text{slip}_{i-2}})$), we form a quadratic approximation of v_{slip} as a function of time:

$$v_{\text{slip}}(t) = at^2 + bt + c, \tag{A.1}$$

where the constants a, b, and c are found by solving the following system of 3 equations in three unknowns:

$$\begin{bmatrix} \tau_i^2 & \tau_i & 1 \\ \tau_{i-1}^2 & \tau_{i-1} & 1 \\ \tau_{i-2}^2 & \tau_{i-2} & 1 \end{bmatrix} \begin{bmatrix} a \\ b \\ c \end{bmatrix} = \begin{bmatrix} v_{\text{slip}_i} \\ v_{\text{slip}_{i-1}} \\ v_{\text{slip}_{i-2}} \end{bmatrix} \tag{A.2}$$

We then find the time, τ^*, when the minimum of this quadratic occurs (i.e. when $dv_{\text{slip}}/dt = 0$) and is given by $\tau^* = -b/2a$. We then integrate one time step from τ_{i-1} to τ^*. If the slip velocity at $t = \tau^*$ has a magnitude that is less than the integration tolerance we then take τ^* as the transition time. Otherwise, we form successive quadratic approximations of v_{slip} as above, each time replacing the point with the largest slip velocity magnitude with the newest point, until the newest slip velocity is less than the integration tolerance.

A.4 Procedure for Finding a Periodic Motion

We find the steady state of the rower-boat-oars system for given coordination splines using an iterative process. Because periodicity only depends on the choice of initial boat velocity, the process of finding a periodic motion is simply a one-dimensional root find. The function whose root we seek, g, is the

difference between the initial and final boat velocities over a stroke. That is, we seek the value of v which makes $g(v) = V - v = 0$ where $v = v_{\mathrm{b}}(0)$ is the boat velocity at $t = 0$ and $V = v_{\mathrm{b}}(T)$ is the boat velocity at $t = T$. The root finding is carried out using a secant method. Starting with an initial boat velocity, v_1, we integrate for two consecutive strokes. The initial boat velocity used for the second stroke, v_2, is the boat velocity at $t = T$ for the first stroke (i.e. $v_2 = V_1$). If $|g_i| = |v_i - V_i|$ is less than the integration tolerance, we determine that steady state has been reached. If not, which is usually the case, we use the points (v_1, g_1) and (v_2, g_2) to construct a linear approximation of $g(v)$:

$$g(v) = \frac{g_2 - g_1}{v_2 - v_1}(v - v_2) + g_2. \tag{A.3}$$

The next guess to the initial boat velocity is then found by determining the root of the linear approximation given by

$$v_3 = v_2 - g_2 \frac{g_2 - g_1}{v_2 - v_1}. \tag{A.4}$$

We then check the value of $|g_3| = |v_3 - V_3|$ to determine whether steady state has been reached. If not, further linear approximations of g are formed until $|g_i|$ is less than the integration tolerance. The procedure normally requires 5 or 6 iterations to make $|g_i| < 10^{-6}$. A numerically slower method would be to integrate forward in time over many strokes until steady-state is accurately-enough reached.

A.5 Measurement Techniques and Data Analysis

A radio telemetry system was used for data acquisition. The system had 12 bit resolution, 32 channels, and the sampling frequency was 51.9 Hz. The data was telemetered from the rowing boat to the motor-boat, where it was collected in real time using a notebook PC (Compaq N800w).

The oar angles in horizontal and vertical planes were measured using servo potentiometers (Bourns 6538, linearity 1%) connected with a light arm and bracket to the oar shaft (Kleshnev, 1999). Force applied to the oar handle was defined by means of measurement of the oar shaft deflection using removable strain-gauges connected in a Wheatstone bridge (Vishay Micro-Measurements 250BB, accuracy ±0.5%). Each oar was calibrated with a force applied 0.06 m from the handle top for sculling and 0.15 m for sweep rowing. Boat velocity was measured using a micro-impeller (Nielsen-Kellerman Co.). Seat position was measured using a multi-turn potentiometer (Bourns 3540, linearity 0.25%)

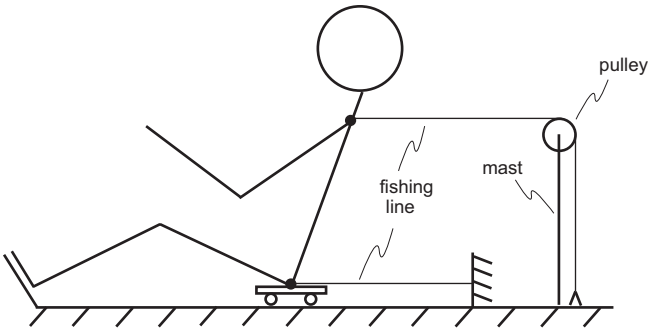

Fig. A.1. Shown is a sketch of the setup used to collect seat slide and back position data. In the case of fours, back position data was not collected due to the difficulty in setting up the equipment.

connected to the seat with low stretchable fishing line. The position of the top of the trunk was measured using the same potentiometer as for the seat position (Kleshnev, 2000). The device was attached to the boat deck and the fishing line went through a pulley mounted on a mast and attached to the trunk at the level of the joint *Sternum* and *Clavicle* (C7). See Fig. A.1 for a schematic of the setup used to measure seat and trunk position. Note that trunk position was not measured for fours due to the difficulty in connecting the fishing line to the middle rowers. The total masses of the data acquisition system including sensors, cables, and electronics were 3.9 and 6 kg for singles and fours, respectively.

The average stroke period and its standard deviation are calculated over several cycles in the sample. Cycles deviating from the average by more than three standard deviations (plus or minus) are excluded. After the filtering described above, each cycle is normalized in time, i.e. stretched or compressed to make each cycle time equal to the average cycle time. The moment when the right oar crossed zero angle value during recovery is chosen as the cycle start. Each cycle time is then divided into 50 equal time intervals. Values at the start of the cycle and at the end of these intervals are calculated from the raw data using cubic interpolation. These values are then averaged over the sample period. The amount of points per stroke cycle (50) was chosen as a compromise between data accuracy and volume.

A.6 Quantification and Minimization of Difference Between Model and Data

Given model parameters we can solve the governing equations to a high numerical accuracy (say, 1 part in 10^{-6}) for the prediction of all force and motion quantities. Similarly, we can imagine that we have precise data for the same quantities measured for a real boat with real people. The error in our pre-

diction of the forces and motions for given model values for the coordination pattern, $\mathbf{u}(t)$, can be quantified using the following function, J_0, describing the net error in the various curve predictions:

$$\text{Measure of fit-error} = J_0[\mathbf{u}(t)] = \frac{\sum_{j=1}^{n_m} w_j E(Y_j)}{\sum_{j=1}^{n_m} w_j}, \tag{A.5}$$

where

- $\mathbf{u}(t) = (\tilde{x}_{\mathrm{B/F}}(t), \tilde{x}_{\mathrm{S/B}}(t), \tilde{x}_{\mathrm{H/S}}(t))$ is the list of body displacements as functions of time,
- n_m is the number of measured variables to be fit,
- $Y_j[\mathbf{u}(t), t]$ is the *simulated* value of variable j and is a function of the coordination and (possibly) time,
- $\hat{Y}_j(t)$ is the *measured* value of variable j and is a function of time,
- w_j are weights in the error assessment,
- $E(Y_j) = (1/T) \int_0^T (Y_j[\mathbf{u}(t), t] - \hat{Y}_j(t))^2/(Y_j^*)^2 dt$ is the weighted error contribution to J_0 for the variable Y_j, and
- Y_j^* is a characteristic value of variable j.

The integrals in J_0 are commonly referred to as the "L^2-norms" of the dimensionless residuals, $(Y_j[\mathbf{u}(t), t] - \hat{Y}_j(t))/Y_j^*$. We use the average boat velocity, peak oar handle force, and peak-to-peak amplitudes of seat slide, oar angle, and back position as the characteristic values, Y_j^*. We also use equal weights, $w_j = 1$ for all j, in the error assessment. Note that $\sum E(Y_j) \approx 1$ if all errors are about as big as the curve magnitudes.

We cannot measure the forces and motions in a continuous manner and the governing equations cannot be solved exactly. Therefore, we can only obtain an approximation of J_0 which we find by evaluating its discretized form in which the Y_j are determined by numerical integration of the equations of motion and in which the integrals become summations of the squares of the residuals over the discrete data points. The new objective function, J, is then:

$$J_0(\mathbf{u}) \approx J(\mathbf{p}) = \frac{\sum_{j=1}^{n_m} w_j E(Y_j)}{N \sum_{j=1}^{n_m} w_j}, \tag{A.6}$$

where

- $\mathbf{p} = (p_1, \ldots, p_{3(n-1)+1})$ is the vector of spline knots defining the coordination and the oarlock fore-aft positioning,
- N is the number of data points collected for each variable,
- Y_{ij} is the *simulated* value of variable j at time step i,
- $\hat{Y}_{ij}$ is the *measured* value of variable j at time step i, and

- $E(Y_j) = (1/N)\sum_{i=1}^{N}(Y_{ij}(\mathbf{p}) - \hat{Y}_{ij})^2/(Y_j^*)^2$ is the weighted error contribution to J for the variable Y_j.

The overall goal in choosing the form of J is to ensure that the computed error has the following invariance properties:

(1) If the errors in each curve are the same (i.e. $\sum E(Y_j)$ is the same for all j) then the value of J does not depend on how many variables we include in the fit (n_m).
(2) For each fitted variable, j, if the residuals are the same for each measurement ($Y_{ij} - \hat{Y}_{ij}$ is the same for all i) then the value of J does not depend on how many data points we have (N).
(3) The value of J does not change if we scale the weights, w_j, by a constant.

Although $3n+1$ parameters define the coordination and oarlock fore-aft position, we only have $3(n-1)+1$ free parameters in the minimization procedure. The reason for this reduction from $3n+1$ to $3(n-1)+1$ parameters is as follows. Since we do not have measurements of the initial leg and back position ($x_{\mathrm{B/F}}(0)$ and $x_{\mathrm{S/B}}(0)$) we fix these values to be constant, reducing the number of free parameters by 2. We obtain a further reduction by considering the equation defining the oar angle:

$$\begin{aligned} s\sin\theta &= d_{\mathrm{L/F}} + x_{\mathrm{H/S}}(t) - x_{\mathrm{S/B}}(t) - x_{\mathrm{B/F}}(t), \\ &= d_{\mathrm{L/F}} + x_{\mathrm{H/S}}(0) + \tilde{x}_{\mathrm{H/S}}(t) - x_{\mathrm{S/B}}(0) - \tilde{x}_{\mathrm{S/B}}(t) - \\ &\quad x_{\mathrm{B/F}}(0) - \tilde{x}_{\mathrm{B/F}}(t), \end{aligned} \tag{A.7}$$

The values of $x_{\mathrm{B/F}}(0)$ and $x_{\mathrm{S/B}}(0)$ are now fixed but we still have $d_{\mathrm{L/F}}$ and $x_{\mathrm{H/S}}(0)$ as free parameters. However, we cannot choose these latter two parameters independently. That is, if we want the sum of these values to equal 1, there are an infinite number of choices of ($d_{\mathrm{L/F}}$,$x_{\mathrm{H/S}}(0)$) pairs to make this happen. Therefore, we fix $x_{\mathrm{H/S}}(0)$ and allow $d_{\mathrm{L/F}}$ to be free (equivalently, we could fix $d_{\mathrm{L/F}}$ and let $x_{\mathrm{H/S}}(0)$ be free) giving us 1 less free parameter. Thus, we have $3(n-1)$ parameters defining the body displacements (since the initial positions are now fixed) and 1 additional parameter defining the oarlock fore-aft positioning.

In Section 4.1, we penalize roughness in the coordination by minimizing J^*:

$$J^*(\mathbf{p}) = (1-\lambda)J(\mathbf{p}) + \lambda \int_0^T ([\ddot{x}_{\mathrm{B/F}}(t)]^2 + [\ddot{x}_{\mathrm{S/B}}(t)]^2)\, dt, \tag{A.8}$$

where $\lambda = 5 \times 10^{-5}$ determines the relative weight between model error and coordination roughness.

Using the integration step size $h = T/(2 \times N)$ and an arbitrary $\mathbf{p}$, we are able to calculate J to within an absolute *numerical* error of 10^{-8}. Because typical values of J are 10^{-3}, J is calculated with a precision of about 1 part in 10^{-5}.

We find the best fits to the data by searching for the set of parameters, $\mathbf{p}$, that minimize J. The optimization problem is solved using a quasi-Newton method with a line search. Gradients of the objective function are computed using forward differencing with a step size of 10^{-7} for all variables. A careful investigation of the accuracy of these gradient calculations show that this step size results in relative errors on the order of not more than 10^{-5} for all derivatives. The Broyden-Fletcher-Goldfarb-Shanno (BFGS) update (outlined in Nocedal & Wright (1999)) is used to approximate the Hessian of the objective function and a quadratic-cubic polynomial line search (also outlined in Nocedal & Wright (1999)) is implemented to determine an appropriate step in the 'search direction', i.e. the vector given by the inverse (approximate) Hessian multiplied by the gradient of J. The minimization is terminated when the magnitude of the dot product of the gradient with the 'search direction' vector is less than 50×10^{-8}.

A.7 How $J_{\min}$ Varies with n

For each n (number of knots used to define the coordination splines) we find best fits to the data for fours and singles by picking the values of the knot ordinates describing the body displacement curves and the oarlock fore-aft positioning that minimize J. All other parameters are fixed to their values as given in Table 2.7. We fit for all of the data ($n_m = 4$ for fours and $n_m = 5$ for singles) and for only three of the measured variables for fours. We start with $n = 3$ and increment n by 1 until we reach $n = 10$ after which n is incremented by 2 until we reach $n = 30$. The initial seed for the $n = 3$ case is randomly generated. Initial seeds for subsequent values of n are generated by interpolating the resulting coordination patterns from the previous minimization and using the resulting fore-aft oarlock positioning. Plots of the logarithm (base 10) of $J_{\min}$ versus n are shown in Fig. A.2 for both singles and fours using both models for the oar blade force. The fits naturally tend to get better as the parameterization grid is refined beyond $n = 8$. In the case when we only fit three of the measured variables for fours, the variables we fit are v_{b}, θ, and $x_{\mathrm{B/F}}$. We notice in Fig. A.2 that the value of $J_{\min}$ is smaller for $n_m = 3$ than it is for $n_m = 4$ for all n. We also notice in this case that $J_{\min}$ decreases more rapidly as n is increased. When $n_m = 3$ and we choose $n = 50$ we should be able to obtain exact fits to the data since there are 50 data points for each measured variable. This case is not shown in the plot but we obtain an objective function value of 1.62×10^{-5}. The fact that we do not obtain zero in this case (to within the accuracy of the calculation of J) is due to the imperfect

convergence of the curve-fit optimization.

In the plot of $J_{\min}$ versus n using Model 1, it appears that $J_{\min}$ begins to level off at about $n = 16$. So we use 16 parameters to define each coordination spline for all subsequent investigations.

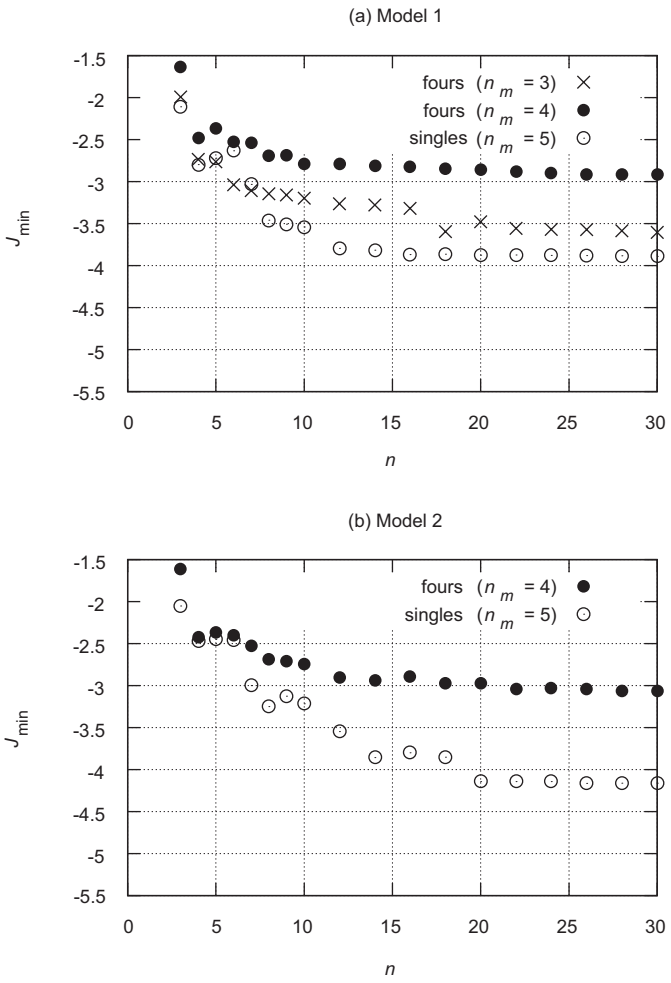

Fig. A.2. Plots of $J_{\min}$ versus the number of knots used in each body position curve using (a) Model 1 and (b) Model 2 for the oar blade force. Here, we are fitting all of the measured variables.

References

Alexander, F. H. (1925). The theory of rowing. *Proceedings of the University of Durham Philosophical Society*, (pp. 160–179).

Atkinson, W. (2004). Rowing computer research. Retrieved Feb. 1, 2005 from the World Wide Web: http://www.atkinsopht.com/row/rowrpage.htm .

Brearley, M. N., & de Mestre, N. J. (1996). Modeling the rowing stroke and increasing its efficiency. In *Proceedings of the 3rd Conference on Maths and Computers in Sport*, (pp. 35–46). Bond University.

Brearley, M. N., & de Mestre, N. J. (1998). The effect of oar flexing on rowing performance. In *Proceedings of the 4th Conference on Maths and Computers in Sport*, (pp. 21–32). Bond University.

Cabrera, D. S. (2005). *Investigations of Rowing Mechanics*. PhD Thesis. Cornell University.

Fox, R. W., & McDonald, A. T. (1992). *Introduction to Fluid Mechanics,*

Fourth Edition. New York: John Wiley and Sons, Inc.

Hoerner, S. F. (1965). *Fluid-dynamic drag*. New York: S. F. Hoerner.

Kleshnev, V. (1999). Propulsive efficiency of rowing. In *Proceedings of the XVII International Symposium on Biomechanics in Sports*, (pp. 224–228). Edith Cowan University, Perth, Western Australia.

Kleshnev, V. (2000) Power in rowing. In *Proceedings of the XVIII International Symposium on Biomechanics in Sports*, (pp. 662–666). The Chinese University of Hong Kong.

Lazauskas, L. (1997). A performance prediction model for rowing races. Technical report, University of Adelaide, Australia. http://www.cyberiad.net/rowing.htm

Lazauskas, L. (1998). Rowing shell drag comparisons. Technical report, University of Adelaide, Australia. http://www.cyberiad.net/rowing.htm

Lighthill, J. (1986). *An informal introduction to theoretical fluid mechanics*. New York: Oxford.

McLean, S. G., Su, A., & van den Bogert, A. J. (2003). Development & validation of a 3-D model to predict knee joint loading during dynamic movement. *Journal of Biomechanical Engineering*, *125*, 864–874.

McMahon, T. A. (1971). Rowing: A similarity analysis. *Science*, *173*, 349–351.

Millward, A. (1987). A study of the forces exerted by an oarsman and the effect on boat speed. *Journal of Sports Sciences*, *5*, 93–103.

Nocedal, J. & Wright, S. J. (1999). *Numerical Optimization*. Springer-Verlag, New York.

Pope, D. L. (1973). On the dynamics of men and boats and oars. *Mechanics and Sport, ASME*, (pp. 113–130).

Sanderson, B., & Martindale, W. (1986). Towards optimizing rowing technique. *Medicine and Science in Sports and Exercise*, *18*, 454–468.

Simeoni, R. J., Barrett, R., & Manning, J. M. (2002). A new model of rowing based on simple physics. *The Physicist*, *39*, 190–197.

van Holst, M. (2004). On rowing. Retrieved Feb. 1, 2005 from the World Wide Web: http://home.hccnet.nl/m.holst/RoeiWeb.html .

Wang, Z. J., Birch, J., & Dickinson, M. H. (2004). Unsteady forces and vorticity field in hovering flight: two-dimensional computations vs. robotic wing experiments. *Journal of Experimental Biology*, *207*, 449–460.

Wang, Z. J. (2005). Dissecting insect flight. *Annual Review of Fluid Mechanics*, *37*, 183–210.

Wellicome, J. F. (1967). Report on resistance experiments carried out on three racing shells. Technical report, NPL Ship T. M.

Zatsiorsky, V. M. (2002). *Kinetics of Human Motion*. Champaign, IL: Human Kinetics.